Tectonophysics 627 (2014) 193–204

Contents lists available at ScienceDirect

Tectonophysics

journal homepage: www.elsevier.com/locate/tecto

2.5-Dimensional tomography of uppermost mantle beneath Sichuan–Yunnan and surrounding regions

Yan Lü [a,*], Zhongjie Zhang [a], Shunping Pei [b], Eric Sandvol [c], Tao Xu [a], Xiaofeng Liang [a]

[a] Institute of Geology and Geophysics, Chinese Academy of Sciences, Beijing 100029, China
[b] Institute of Tibetan Plateau Research, Chinese Academy of Sciences, Beijing 100085, China
[c] Department of Geological Sciences, University of Missouri, Columbia, MO 65211, USA

ARTICLE INFO

Article history:
Received 19 December 2012
Received in revised form 31 January 2013
Accepted 5 March 2013
Available online 16 March 2013

Keywords:
Uppermost mantle
Tomography
Velocity
Vp/Vs ratio
Subduction
Hot material

ABSTRACT

We examine the Pn and Sn travel time data with long and short epicentral distance ranges separately and obtain 2.5-dimensional tomographic models for the uppermost mantle velocity and the Vp/Vs ratio beneath the Sichuan–Yunnan and adjacent regions. The tomographic models show that the average Vp and Vs of the upper layer are approximately 8.10 km/s and 4.60 km/s and those of the deeper layer are 8.19 km/s and 4.65 km/s, respectively; the average velocity ratio is 1.76 under the study area. A comparison of the Pn and Sn velocity distribution reveals that the high- and low-velocity anomalies are consistent. High velocity and low Vp/Vs ratios exist in the Sichuan Basin and low velocity and high ratios distribute in the Myanmar–Yunnan, Songpan–Ganzi, and Hainan regions, respectively. Our models provide more evidence for the subduction of the Indian plate beneath the Myanmar–Yunnan region and the existence of the hot material upwelling beneath the Hainan region. In our velocity model, there is a significant difference between the southern and the northern parts of the Yunnan region (i.e. north and south of 26° N); we infer that these regions are controlled by different dynamic processes. The velocity distributions at different depths are mainly similar in most of the regions of the study area, and the differences between the upper layer and the deeper layer beneath the Yunnan region indicate that the heat flow from the upper mantle has complex characteristics.

1. Introduction

The Sichuan–Yunnan and surrounding regions include the Sichuan Basin, the Songpan–Ganzi fold belt, the Yungui Plateau, Hainan, Myanmar, and other neighboring areas (Fig. 1). This complex region has been the focus of several investigations (Chen et al., in press; Hu et al., 2012; Lei et al., 2009a, 2009b; Liang et al., 2011; Molnar and Tapponnier, 1975; Pei et al., 2011; Teng et al., 1994; Wu and Zhang, 2012; Yao et al., 2008; Zhang and Klemperer, 2010; Zhang et al., 2005, 2009, 2011, in press). The collision between the Indian and Eurasian plates is the driver for the tectonics of this area. Observations made using global positioning systems reveal that materials from the Tibetan Plateau rotate around the eastern Himalayan syntaxis (Wang et al., 2001). Teleseismic body-wave tomography research has revealed large-scale velocity structure beneath this region (Huang and Zhao, 2006; Li et al., 2008).

Pn tomography can image lateral velocity variations in the uppermost mantle (Al-Lazki et al., 2004; Cui and Pei, 2009; Hearn and Ni, 1994; Hearn et al., 2004; Liang et al., 2004; Pei et al., 2007; Phillips et al., 2007; Ritzwoller et al., 2002). Variations in the composition, temperature, pressure, and volatile content of the uppermost mantle can contribute to the Pn and Sn velocity anomalies. The effect of the temperature change is more pronounced on the S-wave velocity (Vs) than on the P-wave velocity (Vp). In high-temperature regions where partial melting occurs, the S-wave velocity decreases more significantly than the P-wave velocity (Badal et al., 1996; Goes et al., 2000; Nolet and Ziehuis, 1994; Thybo, 2006). Therefore, the Sn velocity and Vp/Vs ratio distribution provide better constraints of thermal anomalies and possible partial melt in the study region.

Pn and Sn rays do not travel strictly at the surface of the mantle but dive into the mantle caused by both the earth's curvature and the positive velocity gradients in the uppermost mantle. Most previous studies have used data with only a short epicenter distance within 10° and developed only one 2D model. Hearn et al. (2004) attempted to use data with different epicenter distances in order to obtain different models; however, restricted by the limited data, he could obtain only the Pn velocity model and not the Sn velocity and Vp/Vs models for different depths. Here, we present the P-wave velocity, S-wave velocity and Vp/Vs ratio tomographic models of layers at different depths for the uppermost mantle beneath the Sichuan–Yunnan and adjacent regions by using a large new dataset. This study provides a 2.5-dimensional velocity structure for both P and S waves of the study area.

* Corresponding author. Tel.: +86 13810346916.
E-mail address: lvyan@mail.iggcas.ac.cn (Y. Lü).

0040-1951/$ – see front matter © 2013 Elsevier B.V. All rights reserved.
http://dx.doi.org/10.1016/j.tecto.2013.03.008

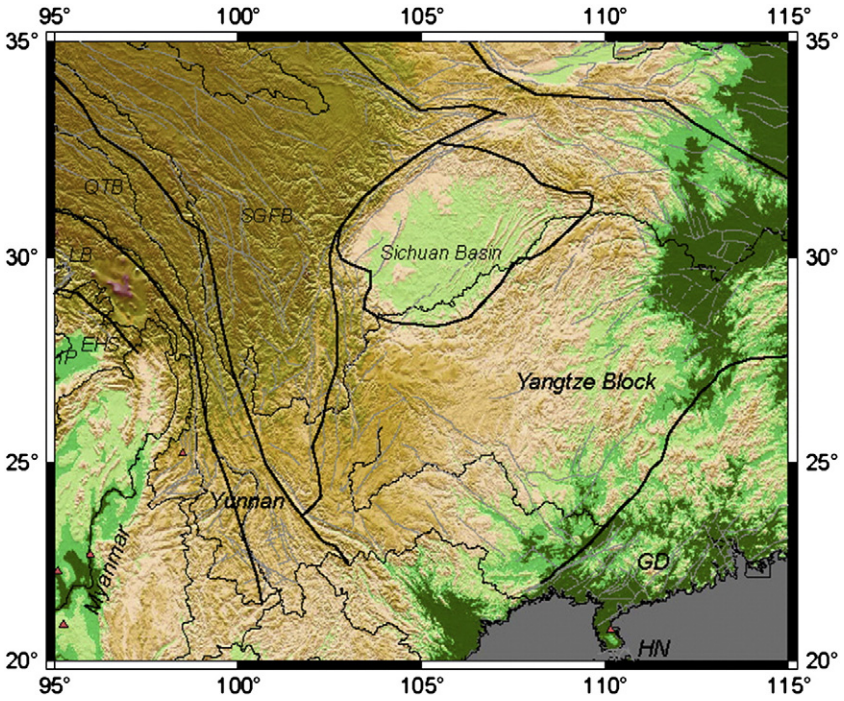

Fig. 1. Simplified tectonic map of Sichuan–Yunnan and surrounding regions superimposed on topography. EHS, eastern Himalayan syntaxis; GD, Guangdong; HN, Hainan; IP, Indian plate; LB, Lhasa Block; QTB, Qiangtang Block; SGFB, Songpan–Ganzi fold belt. Triangles denote volcanoes; black lines represent the tectonic line and the outline of Sichuan Basin; thin gray lines indicate active faults.

2. Data and method

Our study area is located between 20°N and 35°N and between 95°E and 115°E. Seismic data from 10,378 events recorded by 141 stations between 5°N and 50°N, and 80°E and 130°E were used in the study. These travel time data are from three sources, the International Seismological Centre (1960–2007), the China Earthquake Data Center (1990–2009), and the Annual Bulletin of Chinese Earthquakes (1985–2011). Only the Pn and Sn ray pairs that have the same event and station coordinates were used thus making the ray path coverage identical for both Pn and Sn waves. In total, 134,862 rays were used in this study.

Fig. 2 shows the ray paths using a model with a positive P-wave velocity gradient of 0.002 s^{-1} in the upper mantle by segmental iterative ray tracing considering the earth's curvature (Phillips et al., 2007; Xu et al., 2006, 2010). For the inversion, we used the Pn and Sn data for which the epicenter distance ranged between 3° and 10° to obtain the velocity model of the upper layer of the uppermost mantle, and used data for which the epicenter distance ranged between 10° and 16° to obtain the velocity model of the deeper layer of the uppermost mantle. The deeper layer model can represent the lateral variations at the depth of approximately 30–50 km under the Moho discontinuity. Initial models were obtained by a fit to the travel time–distance curve considering the effect of the earth's curvature (Helmberger, 1973; Zhao, 1993). The average Vp and Vs of the upper layer are 8.10 km/s and 4.60 km/s and those of the deeper layer are 8.19 km/s and 4.65 km/s, respectively (Fig. 3). The travel time residuals (difference between predicted and reported travel times) used in the study were limited to a range of ±5 s. The source/station ray paths are shown in Fig. 4. There are 85,173 rays with the epicenter distance ranged between 3° and 10° and 49,689 rays with the epicenter distance ranged between 10° and 16°. Fig. 5 shows the rays hit counts for cells with 0.5° × 0.5° size. The hit counts for most cells of the study area are more than 50.

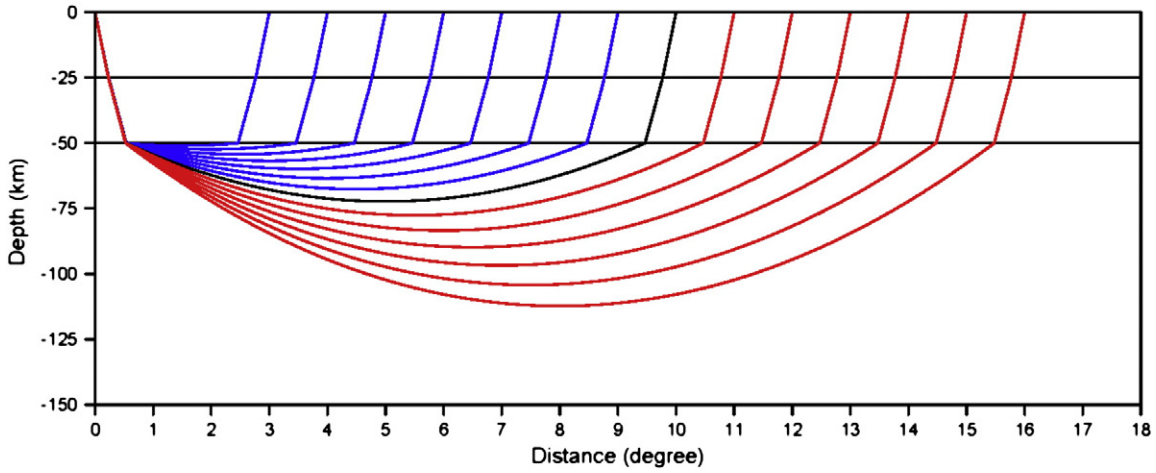

Fig. 2. Ray paths used in a model with positive velocity gradient in upper mantle.

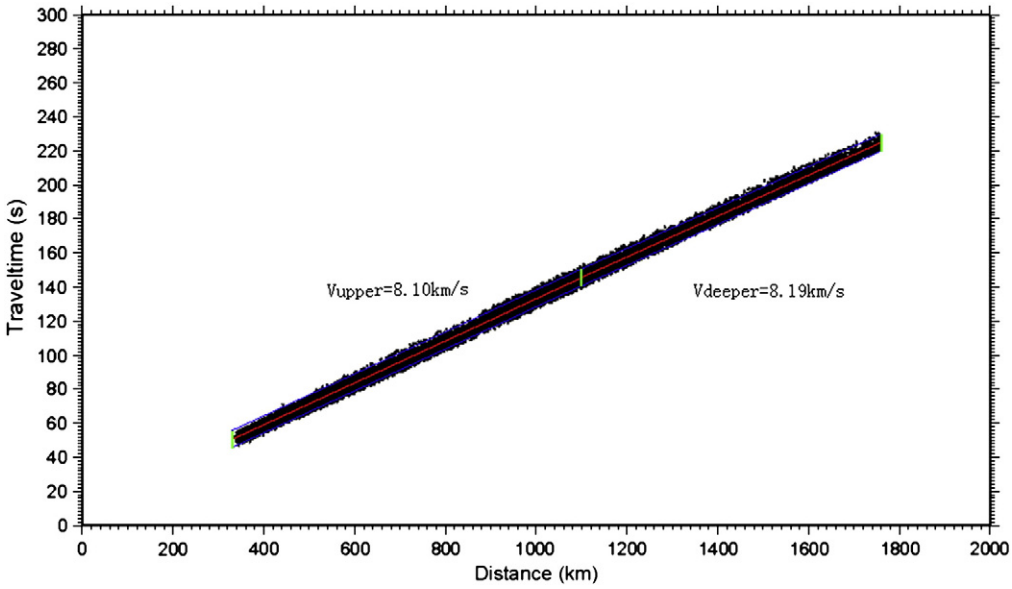

Fig. 3. Distance–travel time curve of the Pn data. The red lines indicate the fitting lines, the blue lines are the quality standard lines, and the green lines indicate the epicenter distance ranges for different layers.

For each layer, we followed the tomography technique developed by Hearn and Ni (1994). The uppermost layer of the mantle is divided into a set of two-dimensional cells, in which the slownesses as same as the inverse velocities are estimated. The travel time residuals are described approximately by the perturbation equation

$$tij = ai + bj + \sum d_{ijk} Sk \quad (1)$$

where t_{ij} is the travel time residual for event j and station i, a_i is the static delay for station i, b_j is the static delay for event j, d_{ijk} is the travel distance of ray ij in mantle cell k, S_k is the slowness perturbation for cell. The unknown quantities in Eq. (1) are the mantle slowness perturbation S_k, the station and event delays a_i and b_j, respectively. The station and event delays accommodate variations in crustal velocity and thickness. The Poisson's ration can be obtained by $\sigma = \frac{(Vp/Vs)^2-2}{2\left[(Vp/Vs)^2-1\right]}$. For the inversion, we used a cell size of 0.5° × 0.5°. The slowness values in each cell were resolved using the LSQR algorithm (Paige and Saunders, 1982; Yao et al., 1999).

While we attempted to resolve azimuthal anisotropy, we could not obtain a sufficient resolution to tightly constrain azimuthal anisotropy fast directions and magnitude. Thus, in this paper, we have focused on the Pn and Sn velocity variations and the velocity ratio, assuming a spatially varying isotropic velocity model. One of the difficulties in measuring Pn and Sn azimuthal anisotropy is the difference in sampling depths for different epicentral distances. Often this requires a relatively narrow range of distances to be used to solve for Pn or Sn anisotropy. Typically including the anisotropic terms, there is only a marginal impact on the major velocity variations (Lü et al., 2011, 2012). Therefore, our tomography most likely can provide a reliable uppermost mantle velocity structure of the study area.

3. Results and discussion

3.1. Resolution tests

Velocity resolution tests were performed in order to determine the size of features that can be reliably imaged, and therefore interpreted. Checkerboard tests were conducted to evaluate the effects of ray coverage on spatial resolution. A test checkerboard velocity model was created by assigning sinusoidal velocity anomalies to the cells of the model domain simultaneously. Synthetic arrival times were calculated for the test model under different checkerboard sizes with the same number of earthquakes, stations, and ray paths that were used for actual tomographic inversion. Gaussian noise with a standard deviation equal to the rms residuals after inversion was added to the synthetic travel times and Gaussian location errors with a standard deviation of 15 km were added to both the latitude and longitude of event locations to simulate the pick errors, hypocenter mislocations, and other noises (Lei et al., 2011). We performed tests using different cell sizes for the sinusoidal velocity anomalies. Fig. 6 shows the checkerboard test results. The spatial resolution is considered to be good for the regions in which the checkerboard pattern is recovered. The tests indicate that, for most of the study region, velocity anomalies with a size of 2.7° × 2.7° can be well resolved, at the western part of the study area, the spatial resolution there can reach 2.0° × 2.0° or even better.

3.2. Upper layer

Fig. 7 shows the Vp and Vs models of the study area by using rays with an epicenter distance of 3°–16° by the traditional way. The average Vp and Vs for the study area are 8.14 km/s and 4.62 km/s, respectively. Low velocities are found to be distributed under the Myanmar–Yunnan region, Hainan region, and the Songpan–Ganzi fold belt; high velocity values are observed beneath the Sichuan Basin. From this integrated model, the main features are the same as the previous result (e.g., Cui and Pei, 2009; Li and Lei, 2012), which can provide 2D velocity information of the uppermost mantle beneath our study area, but cannot provide any depth constraint for the velocity of the uppermost mantle.

Fig. 8 shows the Pn and Sn velocity variations of the upper layer by rays with an epicenter distance of 3°–10°. The average Vp and Vs of this layer for the study area are 8.10 km/s and 4.60 km/s, which are lower than our integrated models (Fig. 7) and reflect the velocity gradient of the uppermost mantle. The average Vp/Vs ratio and Poisson's ratio are approximately 1.76 and 0.262 beneath the study area (Fig. 9). The RMS residuals of the P-wave travel times decreased from 2.0 s to 1.1 s after inversion (Fig. 10A, B), and the residuals of S-wave travel times decreased from 2.2 s to 1.3 s. In general, the variations of the Pn and Sn velocities are similar. High velocity values are observed

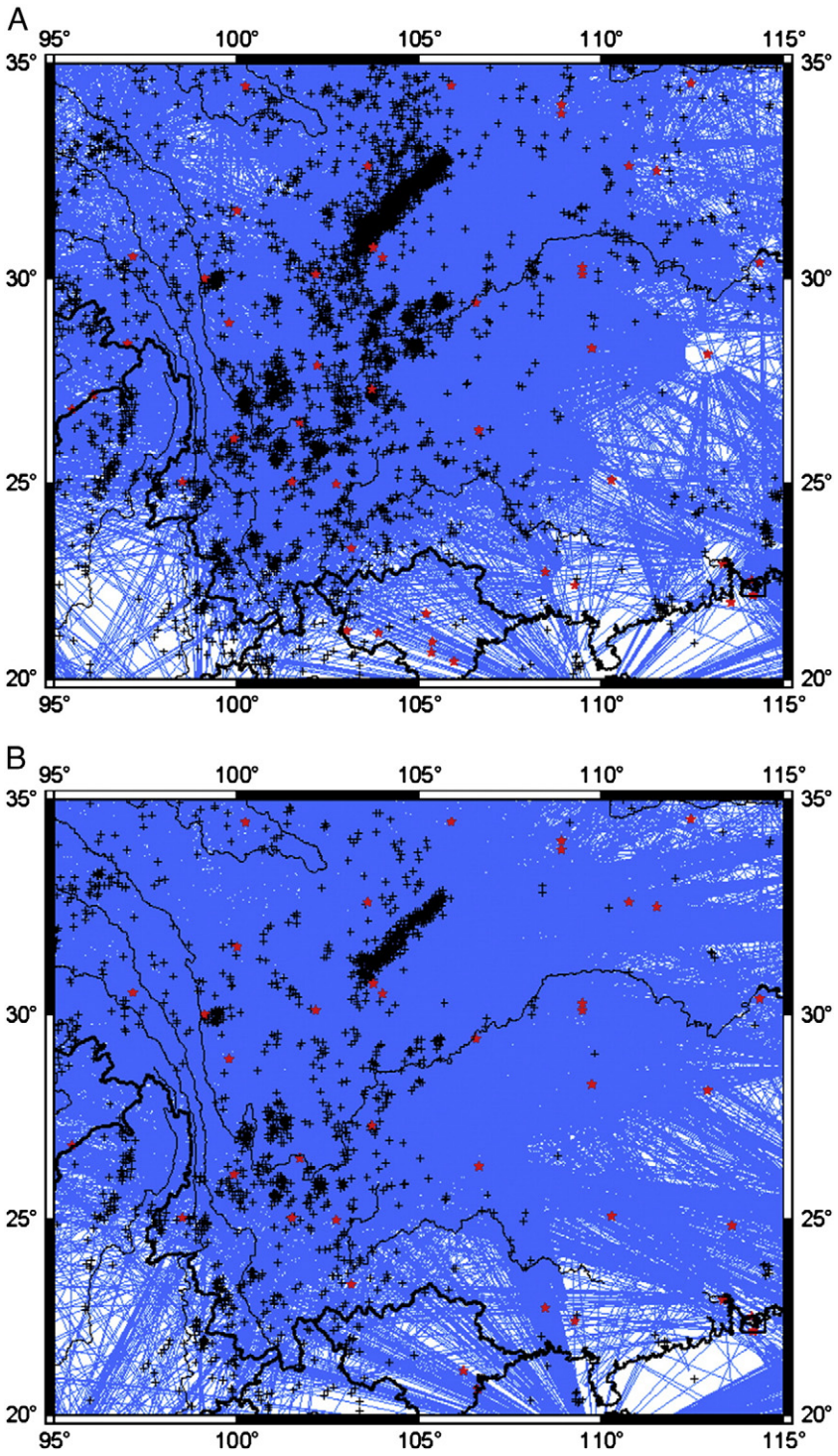

Fig. 4. Ray paths with an epicenter distance ranging between 3° and 10° (A) and with an epicenter distance ranging between 10° and 16° (B). The black crosses represent events, and the red stars indicate stations.

beneath the Sichuan Basin. Clear low velocities are found under the Myanmar–Yunnan region, Hainan region, and the Songpan–Ganzi fold belt.

The model shows that the lithospheres of Sichuan Basin are cold and stable. The stable lithospheres block the material flow from the Tibetan Plateau to the east and change the flow direction to the south. In the Myanmar–Yunnan region, low velocities are distributed around some volcanoes (Lei et al., 2009a). The low velocities in the Myanmar–Yunnan region provide evidence of subduction of the Indian plate eastward and associated back-arc upwelling (Li et al., 2008). In the Hainan region, plume-like low-velocity feature was found in a body-wave tomographic model (Lei et al., 2009b). Our present models also support this observation. The velocity under the Songpan–Ganzi fold belt is significantly low, which has also been observed in previous studies (Lei and Zhao, 2009; Li and Lei, 2012; Li et al., 2010; Liang et al., 2004; Pei et al., 2007, 2010). This low velocity can be primarily attributed to high temperatures, and secondarily to compositional variations due to water (Hearn et al., 2004).

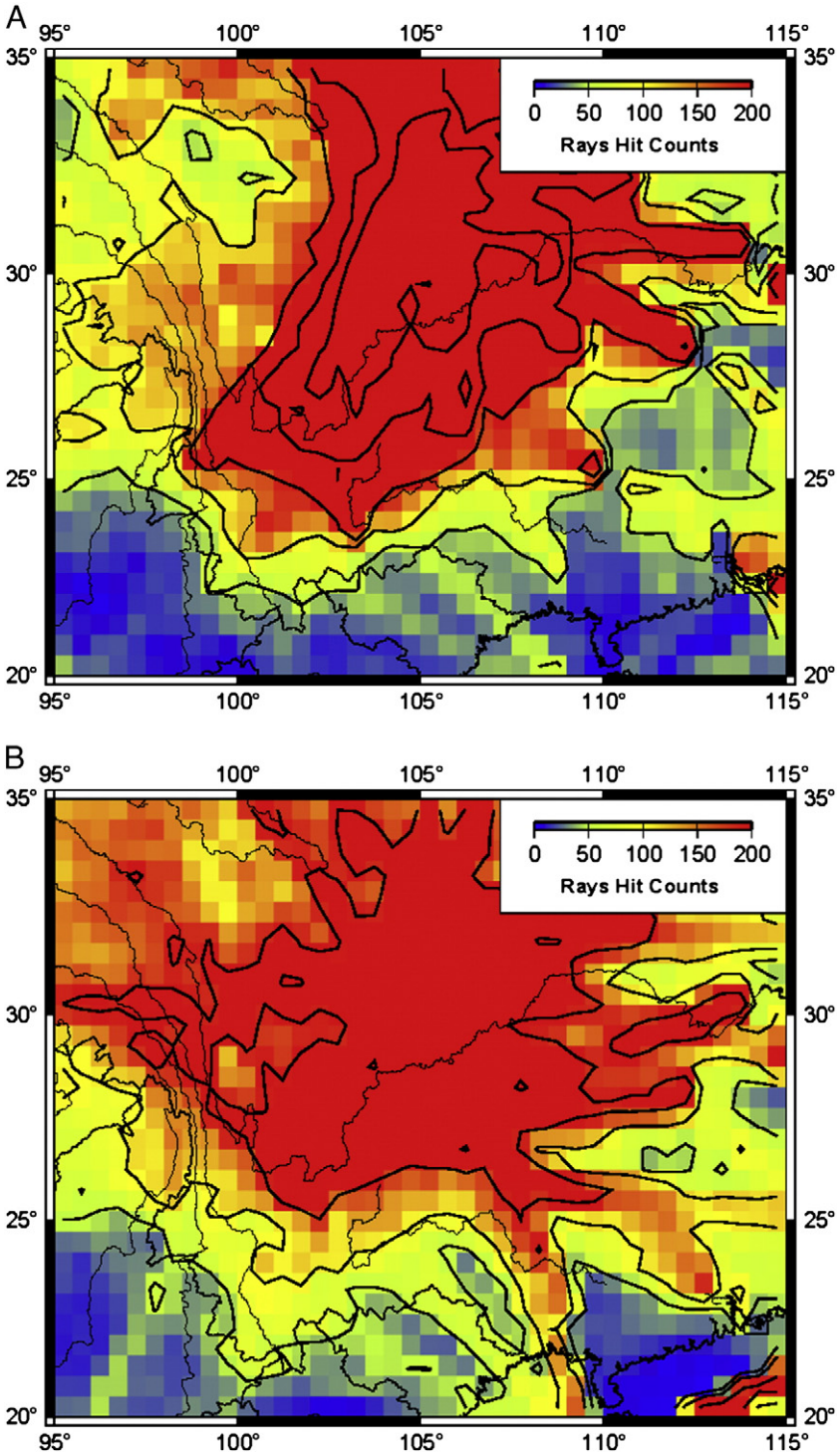

Fig. 5. Hit counts for cells of rays with an epicenter distance ranging between 3° and 10° (A) and with an epicenter distance ranging between 10° and 16° (B). Red and blue correspond to the number of the rays hit counts. The isopleths are pointing 50, 100, 200, 500 and 1000 count number.

3.3. Deeper layer

Fig. 11 shows the Vp and Vs variations of the deeper layer by rays with an epicenter distance of 10°–16°. The average Vp of this layer for the study area is 8.19 km/s, and the average Vs is 4.65 km/s, which are higher than the upper layer (Fig. 8) and the integrated models (Fig. 7). It is clear that as longer epicentral distance data are used, the ray paths sample deeper uppermost mantle, which is the reason why we see a velocity increase for the average velocity of the upper and lower layers and a neutral average velocity for the integrated model. The RMS residuals of P-wave travel times decreased from 2.5 s to 1.5 s after inversion (Fig. 10C, D), and the residuals of S-wave travel times decreased from 2.8 s to 1.7 s.

In general, the Vp and Vs variation patterns are similar to the upper layer model and the integrated model discussed above. High velocity values are observed beneath the Sichuan Basin; low velocities are found to be distributed under the Myanmar–Yunnan region, Hainan region, and the Songpan–Ganzi fold belt. Four independent

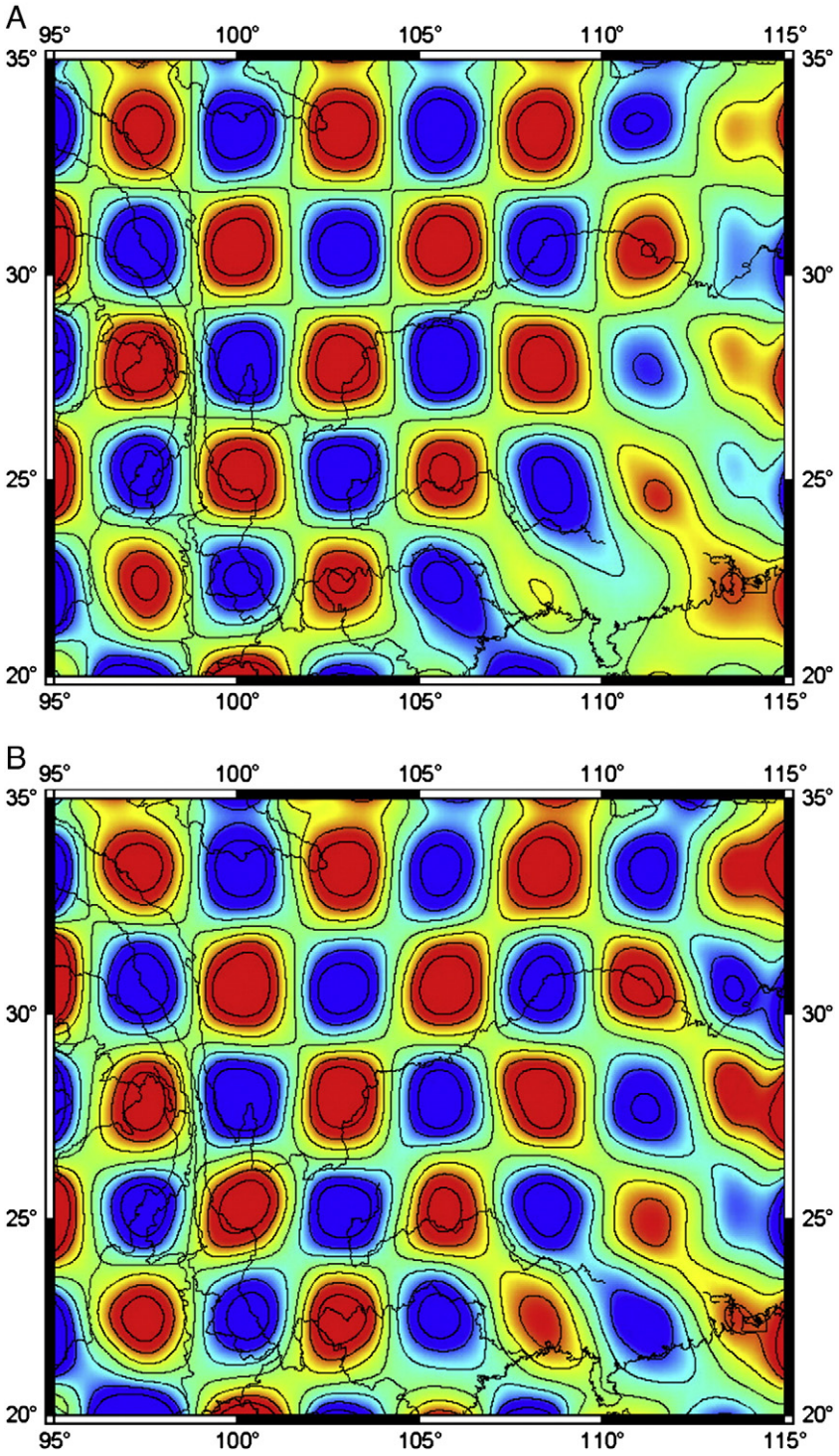

Fig. 6. Checkerboard resolution results for the upper (A) and deeper (B) layers of the model with a cell size of 2.7° × 2.7°.

datasets of the inversion of the Pn and Sn travel time data yielded similar results that are consistent with each other and this confirms the credibility of the inversion results.

A previous study involving an SKS analysis revealed that the fast direction of the shear wave splitting turns from almost N-S direction to W-E direction from north to south around 26° N (Sol et al., 2007). In our model, there is a clear velocity difference between the southern and the northern parts of 26° N in the Yunnan region. Low velocities are found in the southern part of 26° N. Considering the previous SKS splitting and Pn anisotropy results (Cui and Pei, 2009; Li and Lei, 2012), we infer that the southern and the northern parts of 26° N in the Yunnan region are controlled by different dynamic processes. The southern part is mainly affected by the eastern forward subduction of the Indian plate; the northern part is controlled by the material flow from the Tibetan Plateau (Bai et al., 2010; Zhang et al., 2010).

Fig. 12 shows the Vp/Vs ratio distribution. The average Vp/Vs ratio and Poisson's ratio are approximately 1.76 and 0.262 beneath the study area. The velocity ratio distributions are generally similar for both the Vp and the Vs models. The velocity ratio is low in the Sichuan Basin. The very low Vp/Vs ratio beneath the Sichuan block is typical for

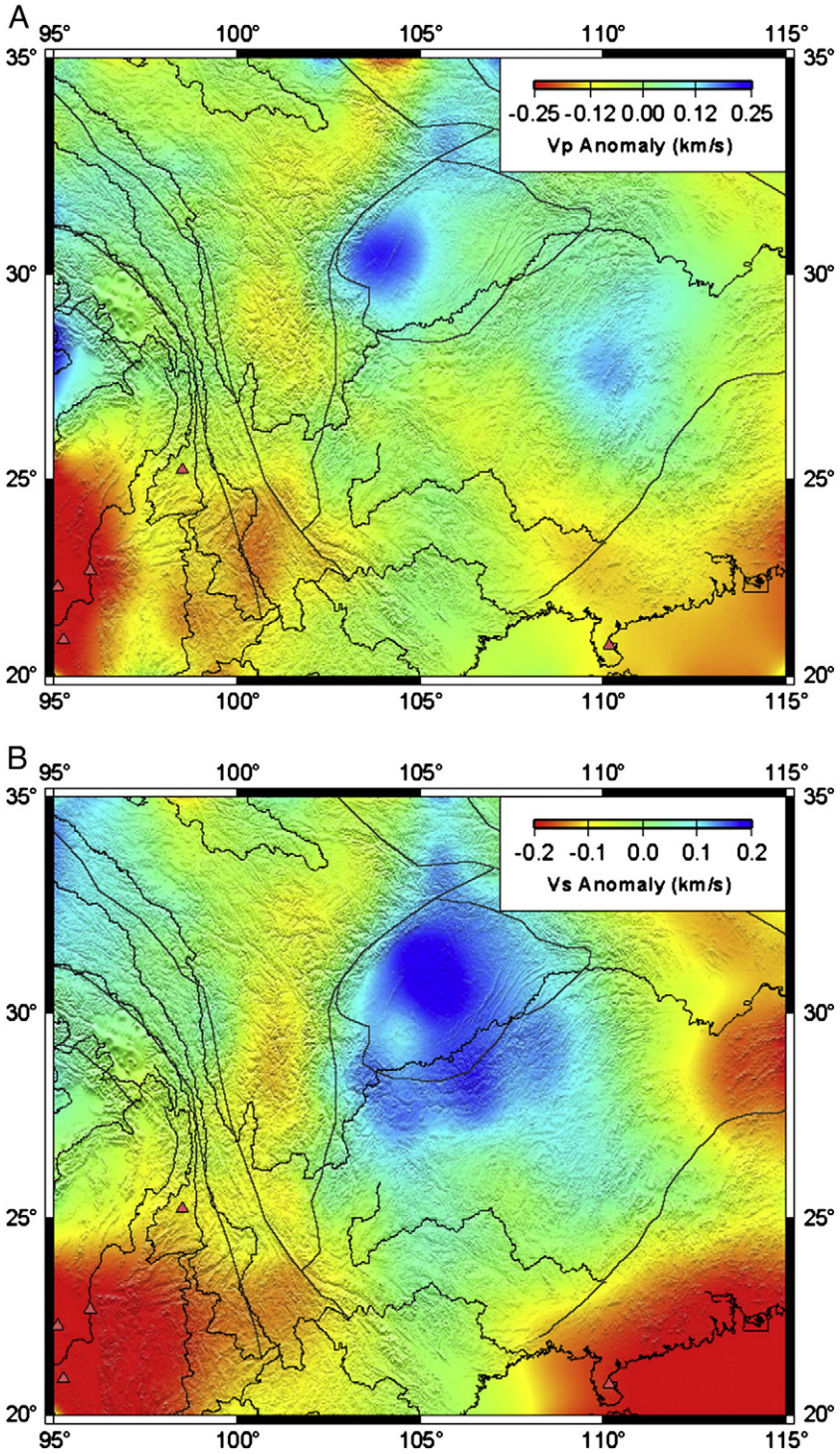

Fig. 7. Lateral Vp (A) and Vs (B) variations inferred from the data with an epicenter distance of 3°–16°. Average Vp is 8.14 km/s, and the average Vs is 4.62 km/s. Red and blue areas correspond to velocities lower and higher than the average, respectively. Triangles denote volcanoes, and the black line represents the tectonic line.

many cratonic regions and can be attributed in part to a depleted lithospheric mantle (Dorbath and Masson, 2000). The average Vp/Vs ratio of our study area is less than the global average for the uppermost mantle which is approximately 1.79 (Christensen, 1996; Rossi et al., 2006), this may be caused by the very low ratio value of the Sichuan region.

In the Myanmar–Yunnan and Hainan regions, the velocity ratio is high, indicating that the uppermost mantle had a high temperature. In the southern part of the Yunnan region, the Vp/Vs ratio distributions are different between the two layers. The velocity ratio at the deeper layer of this region is significantly high nearly 1.80 but which is just around 1.76 at the upper layer. From the heat flow observation (Hu et al., 2001; Wang and Huang, 1990) and crust velocity structure studies (Gao et al., 2009; Wu and Zhang, 2012; Xu et al., 2012), we infer that the hot material upwelling is not straight but more complex beneath the Yunnan region, and the deeper layer is affected by the hot material upwelling considerably seriously.

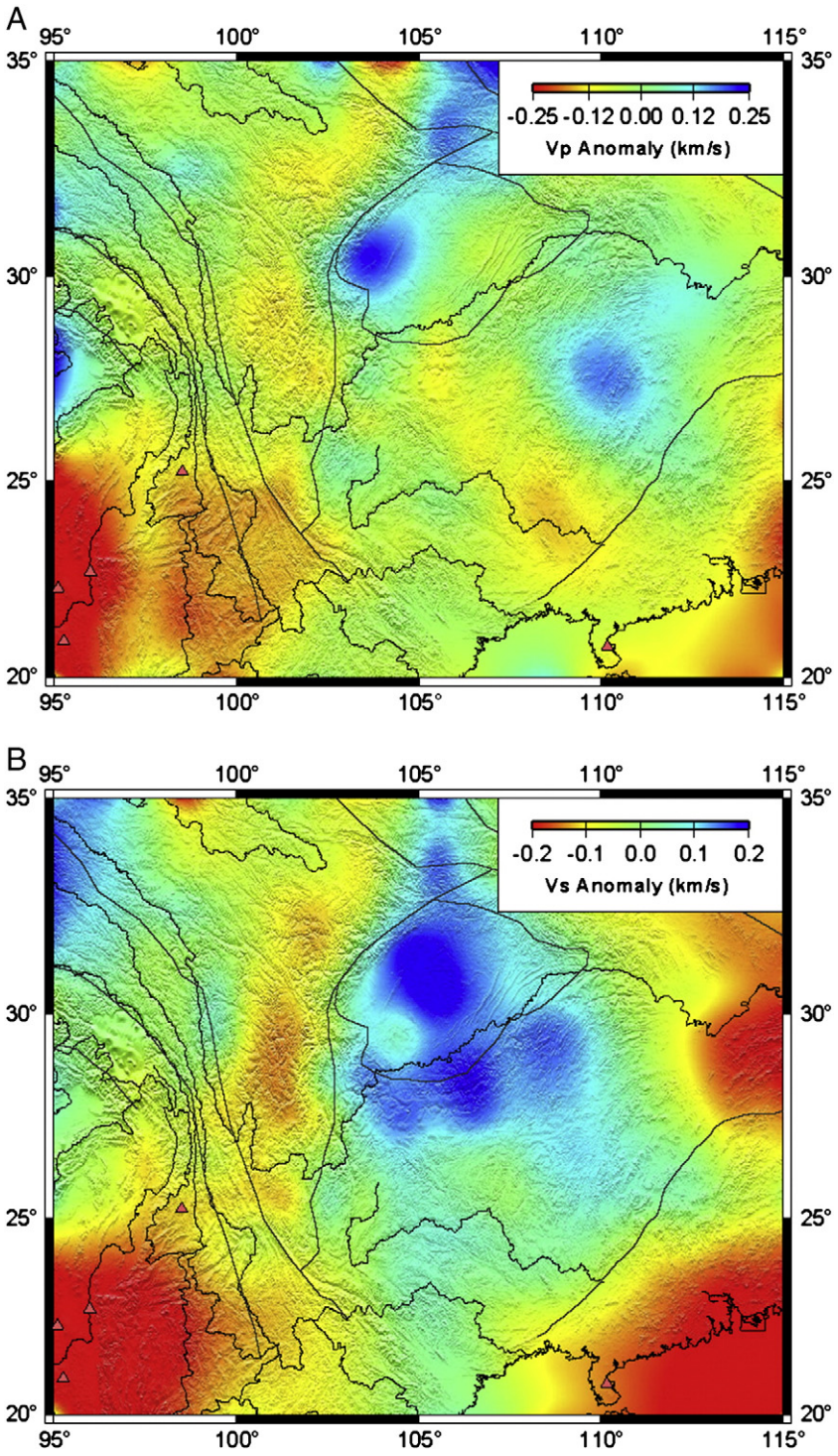

Fig. 8. Lateral Vp (A) and Vs (B) variations for the upper layer. Average Vp is 8.10 km/s, and the average Vs is 4.60 km/s. Red and blue areas correspond to velocities lower and higher than the average, respectively.

4. Conclusions

We examine the Pn and Sn travel time data with long and short epicentral distance ranges separately and obtain 2.5-dimensional tomographic models for the uppermost mantle velocity and the Vp/Vs ratio beneath the Sichuan–Yunnan and adjacent regions. The major conclusions include:

1. In the back-arc region around Myanmar, significant low Vp and Vs are distributed around volcanoes. This is strong evidence to prove that the lithosphere of the Indian plate subducted into the mantle beneath Myanmar and caused the hot material upwelling at the back arc. The high temperature or even partial melting in the uppermost mantle caused the low velocity and the high Vp/Vs ratio.
2. The uppermost mantle velocities of the Sichuan Basin and the Songpan–Ganzi fold belt are considerably different. The high velocities of the Sichuan Basin implied that the lithosphere in this region is stable and cold, which blocked the weaker and likely more ductile material beneath the Songpan–Ganzi terranes

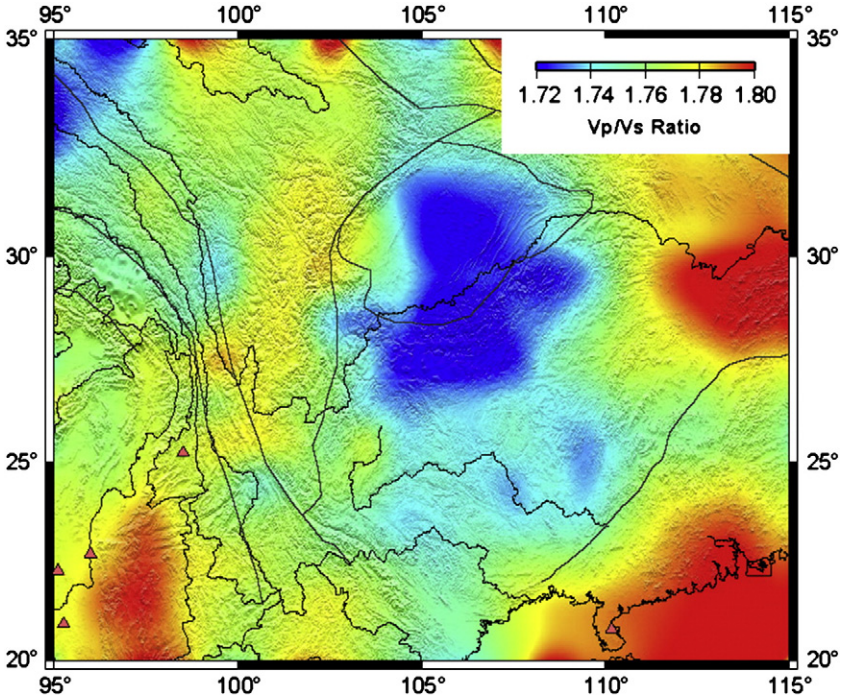

Fig. 9. V_p/V_s ratio variations for the upper layer. Average velocity ratio is 1.76. Red and blue areas correspond to ratios higher and lower than the average, respectively.

flow moving to the east and changed the flow direction to the south. The low velocity in the Songpan–Ganzi region is consistent with that obtained in the previous studies. The very low Vp/Vs ratios beneath the Sichuan block are typical for many cratonic regions and can be attributed in part to a depleted lithospheric mantle.

3. There are significant velocity differences between the southern and the northern parts of 26° N in the Yunnan region. We infer

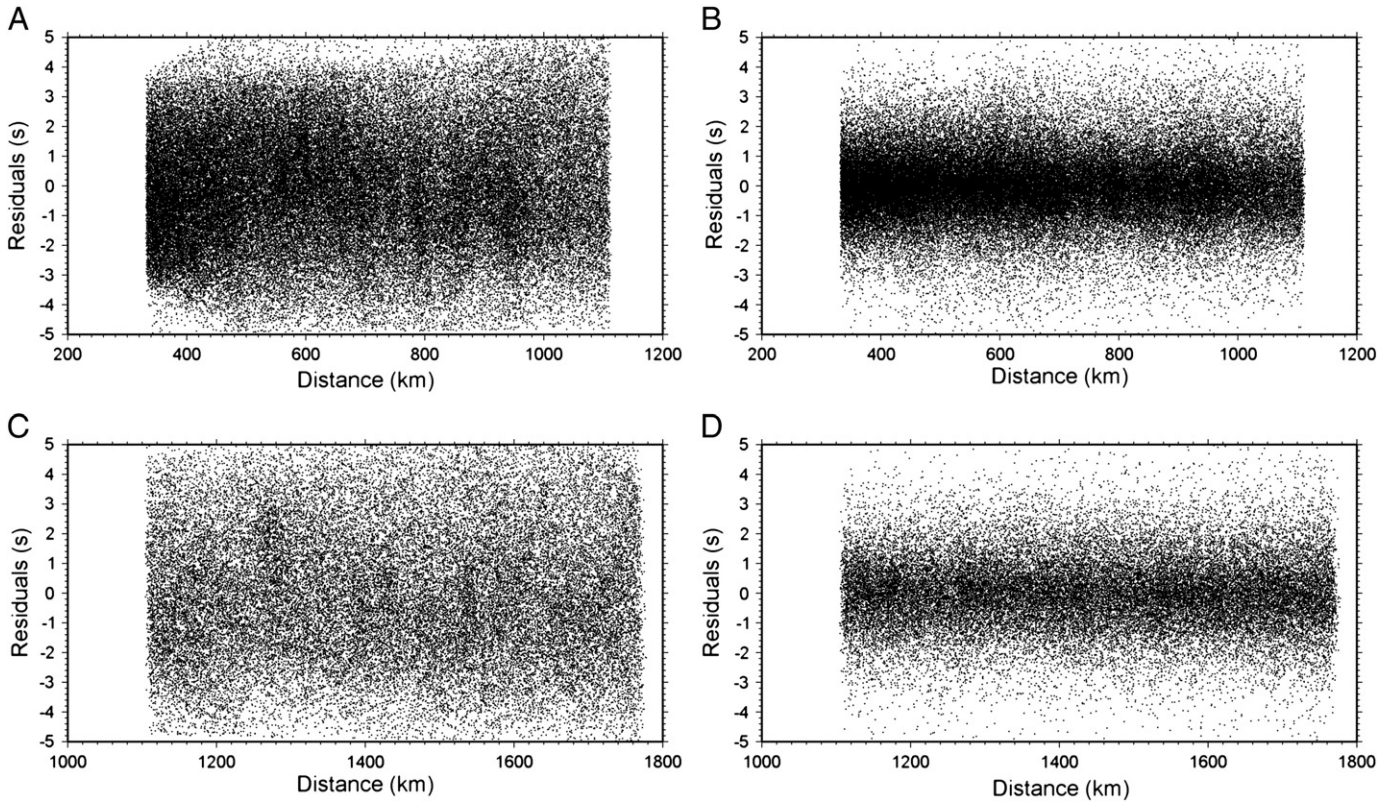

Fig. 10. Distribution of residuals versus epicenter distance before and after inversion for upper layer (A, B) and deeper layer (C, D). The standard deviation of the Pn travel time residuals is 2.0 s and 2.5 s for the original data; it decreases to 1.1 s and 1.5 s after inversion.

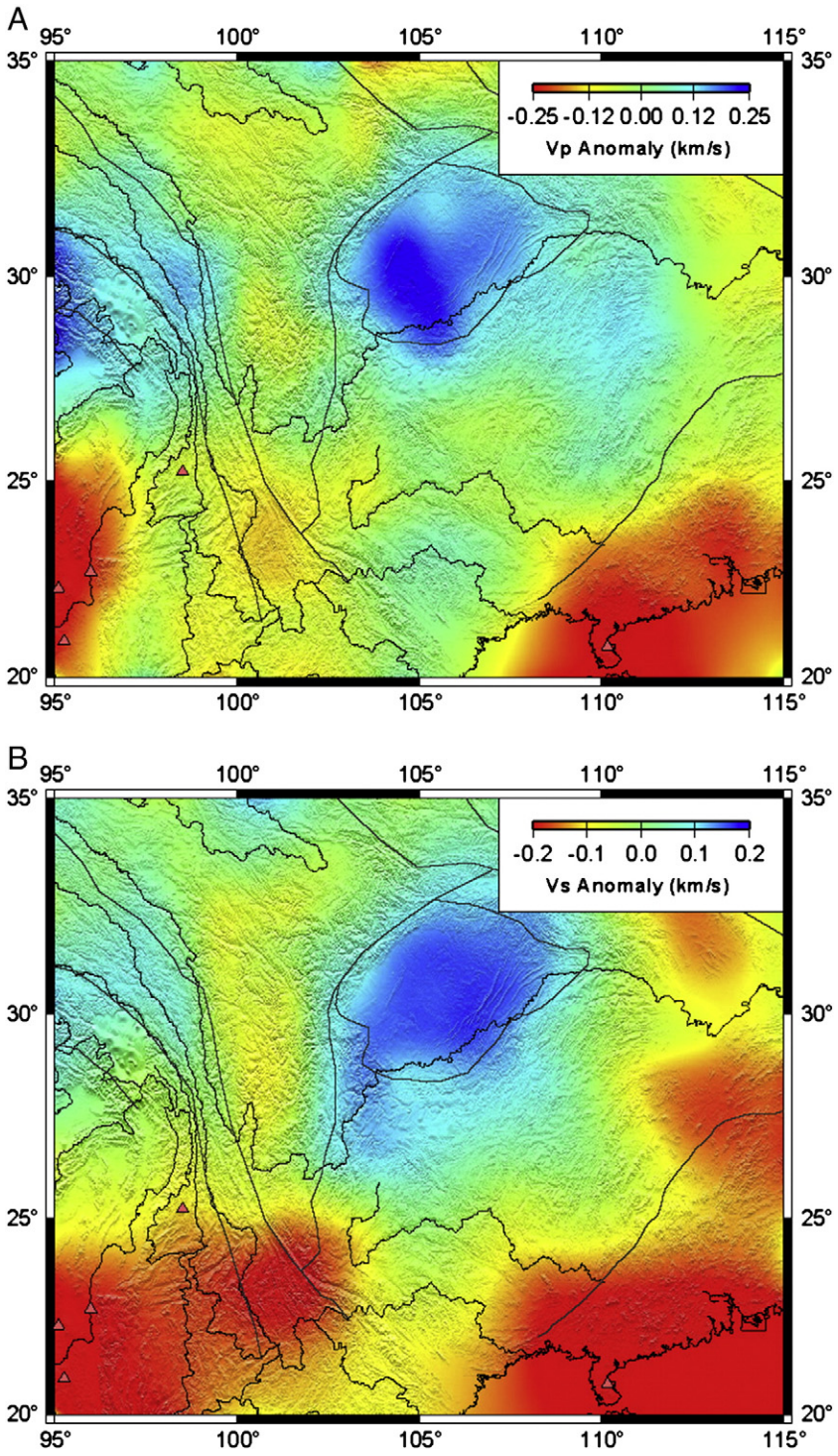

Fig. 11. Lateral Vp (A) and Vs (B) variations for the deeper layer. Average Vp is 8.19 km/s, and the average Vs is 4.65 km/s. Red and blue areas correspond to velocities lower and higher than the average, respectively.

that these parts are controlled by different dynamic processes. The southern part is mainly affected by the eastern forward subduction of the Indian plate, and the northern part is controlled by the material flow from the Tibetan Plateau.

4. The Vp and Vs are low and the Vp/Vs ratio is high in the Hainan region, which is further evidence of the possible mantle plumes beneath the Hainan region. The differences in the velocity ratio distributions between the models of the two layers in the Yunnan region indicate that the hot material upwelling is not straight but more complex and the deeper layer is affected by the hot material upwelling considerably seriously.

Acknowledgments

We would like to thank Thomas M. Hearn for providing the original codes. We thank the suggestions provided by Dr. Juan Li. We appreciate the insightful suggestions by the two reviewers and the editor. Most figures were prepared using the Generic Mapping Tolls

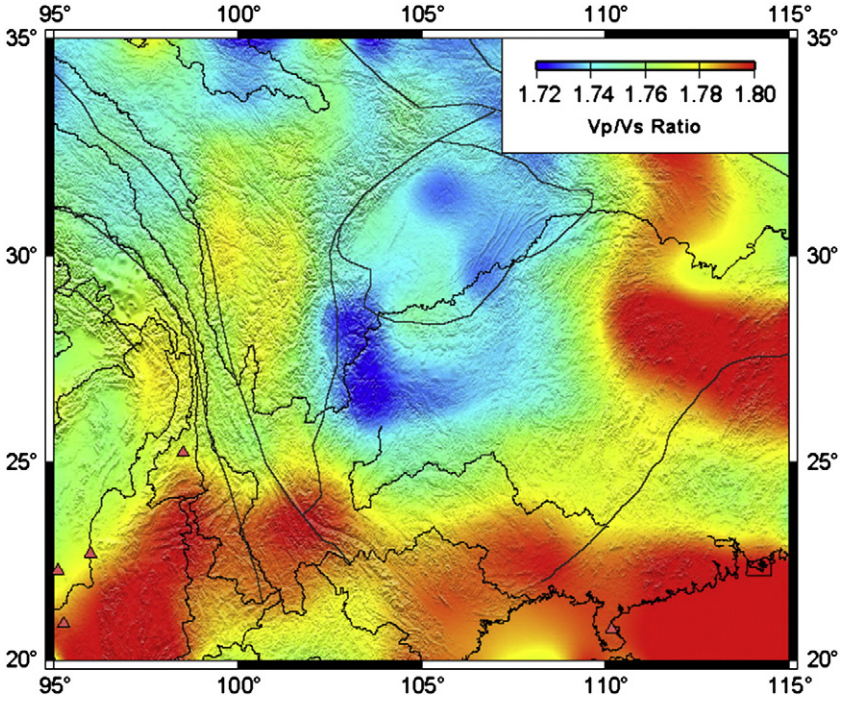

Fig. 12. V_p/V_s ratio variations for the deeper layer. Average velocity ratio is 1.76. Red and blue areas correspond to ratios higher and lower than the average, respectively.

(Wessel and Smith, 1998). This research was supported by the National Nature Science Foundation of China (grant nos. 40830315 and 41021063), the China Postdoctoral Science Foundation 2012M510043 and National Probing Project (SinoProbe-03-02).

References

Al-Lazki, A., Sandvol, E., Seber, D., Barazangi, M., Turkelli, N., Mohamad, R., 2004. Pn tomographic imaging of mantle lid velocity and anisotropy at the junction of the Arabian, Eurasian and African plates. Geophysical Journal International 158, 1024–1040.

Badal, J., Corchete, V., Payo, G., Pujades, L., Canas, J., 1996. Imaging of shear-wave velocity structure beneath Iberia. Geophysical Journal International 2, 591–611.

Bai, D., Unsworth, M., Meju, M., et al., 2010. Crustal deformation of the eastern Tibetan plateau revealed by magnetotelluric imaging. Nature Geoscience 3, 358–362.

Chen, Y., Zhang, Z., Sun, C., Badal, J., in press. Crustal anisotropy from Moho converted Ps wave splitting analysis and geodynamic implications beneath the eastern margin of Tibet and surrounding regions. Gondwana Research. http://dx.doi.org/10.1016/j.gr.2012.04.003.

Christensen, N., 1996. Poisson's ratio and crustal seismology. Journal of Geophysical Research 101, 3139–3156.

Cui, Z., Pei, S., 2009. Study on Pn velocity and anisotropy in the uppermost mantle of the Eastern Himalayan Syntaxis and surrounding regions. Chinese Journal of Geophysics 52, 2245–2254.

Dorbath, C., Masson, F., 2000. Composition of the crust and upper-mantle in the Central Andes (19°30′S) inferred from P wave velocity and Poisson's ratio. Tectonophysics 327, 213–223.

Gao, X., Su, Y., Wang, W., Pei, S., Guo, Z., 2009. Lower-crust S-wave velocity beneath western Yunnan Province from waveform inversion of dense seismic observations. Terra Nova 21, 105–110.

Goes, S., Govers, R., Vacher, P., 2000. Shallow mantle temperatures under Europe from P and S wave tomography. Journal of Geophysical Research 105, 11153–11169.

Hearn, T., Ni, J., 1994. Pn velocities beneath continental collision zones, the Turkish–Iranian plateau. Geophysical Journal International 117, 273–283.

Hearn, T., Wang, S., Ni, J., Xu, Z., Yu, Y., Zhang, X., 2004. Uppermost mantle velocities beneath China and surrounding regions. Journal of Geophysical Research 109, B11301.

Helmberger, D.V., 1973. Numerical seismograms of long-period body waves from seventeen to forty degrees. Bulletin of the Seismological Society of America 63, 633–646.

Hu, S., He, L., Wang, J., 2001. Compilation of heat flow data in the China continental area (3rd edition). Chinese Journal of Geophysics 44, 611–626.

Hu, J., Yang, H., Xu, X., Wen, L., Li, G., 2012. Lithospheric structure and crust–mantle decoupling in the southeast edge of the Tibetan Plateau. Gondwana Research 22, 1060–1067.

Huang, J., Zhao, D., 2006. High-resolution mantle tomography of China and surrounding regions. Journal of Geophysical Research 111. http://dx.doi.org/10.1029/2005JB004066 (B09305).

Lei, J., Zhao, D., 2009. Structural heterogeneity of the Longmenshan fault zone and the mechanism of the 2008 Wenchuan earthquake (Ms 8.0). Geochemistry, Geophysics, Geosystems 10. http://dx.doi.org/10.1029/2009GC002590.

Lei, J., Zhao, D., Su, Y., 2009a. Insight into the origin of the Tengchong intraplate volcano and seismotectonics in southwest China from local and teleseismic data. Journal of Geophysical Research 114. http://dx.doi.org/10.1029/2008JB005881 (B05302).

Lei, J., Zhao, D., Steinberger, B., Wu, B., Shen, F., Li, Z., 2009b. New seismic constraints on the upper mantle structure of the Hainan plume. Physics of the Earth and Planetary Interiors 173, 33–50.

Lei, J., Zhao, D., Xie, F., Liu, J., 2011. An attempt to detect temporal variations of crustal structure in the source area of the 2006 Wen-An earthquake in North China. Journal of Asian Earth Sciences 40, 958–976.

Li, C., Hilst, R.D., Meltzer, A.S., Engdahl, E.R., 2008. Subduction of the Indian lithosphere beneath the Tibetan Plateau and Burma. Earth and Planetary Science Letters 274, 157–168.

Li, H., Su, W., Wang, C., Huang, Z., Lv, Z., 2010. Ambient noise Love wave tomography in the eastern margin of the Tibetan plateau. Tectonophysics 491, 194–204.

Li, Y., Lei, J., 2012. Velocity and anisotropy structure of the uppermost mantle under the eastern Tibetan plateau inferred from Pn tomography. Chinese Journal of Geophysics 55, 3615–3624.

Liang, C., Song, X., Huang, J., 2004. Tomographic inversion of Pn travel times in China. Journal of Geophysical Research 109. http://dx.doi.org/10.1029/2003JB002789 (B11304).

Liang, X., Shen, Y., Chen, Y., Ren, Y., 2011. Crustal and mantle velocity models of southern Tibet from finite frequency tomography. Journal of Geophysical Research 116. http://dx.doi.org/10.1029/2009JB007159 (B02408).

Lü, Y., Ni, S., Liu, B., Sun, Y., 2011. Pn tomographic velocity and anisotropy beneath the Tibetan Plateau and the adjacent regions. Earth, Planets and Space 63, 1169–1173. http://dx.doi.org/10.5047/eps.2011.07.013.

Lü, Y., Liu, B., Pei, S., Sun, Y., Toksöz, M., Zeng, X., 2012. Pn tomographic velocity and anisotropy beneath the Iran region. Bulletin of the Seismological Society of America 102, 426–435. http://dx.doi.org/10.1785/0120100141.

Molnar, P., Tapponnier, P., 1975. Cenozoic tectonics of Asia: effects of a continental collision. Science 18, 419–426.

Nolet, G., Ziehuis, A., 1994. Low S velocities under the Tomquist Teisseyre zone: evidence for water injection into the transition zone by subduction. Journal of Geophysical Research 99, 15813–15820.

Paige, C., Saunders, M., 1982. LSQR, An algorithm for sparse linear equations and sparse linear system. ACM Transactions on Mathematical Software 8, 43–71.

Pei, S., Zhao, J., Sun, Y., et al., 2007. Upper mantle seismic velocities and anisotropy in China determined through Pn and Sn tomography. Journal of Geophysical Research 112. http://dx.doi.org/10.1029/2006JB004409 (B05312).

Pei, S., Su, J., Zhang, H., Sun, Y., Toksöz, M., et al., 2010. Three-dimensional seismic velocity structure across the 2008 Wenchuan Ms 8.0 earthquake, Sichuan, China. Tectonophysics 491, 211–217.

Pei, S., Sun, Y., Toksöz, M., et al., 2011. Imaging Poisson's ratio of the uppermost mantle beneath China. Bulletin of the Seismological Society of America 101, 1452–1461.

Phillips, W., Begnaud, M., Rowe, C., Steck, L., Myers, S., Pasyanos, M., Ballard, S., 2007. Accounting for lateral variations of the upper mantle gradient in Pn tomography studies. Geophysical Research Letters 34. http://dx.doi.org/10.1029/2007GL029338 (L14312).
Ritzwoller, M.H., Barmin, M.P., Villasenor, A., Levshin, A.L., Engdahl, E.R., 2002. Pn and Sn tomography across Eurasia to improve regional seismic event locations. Tectonophysics 358, 39–55.
Rossi, G., Abers, G., Rondenay, S., Christensen, D., 2006. Unusual mantle Poisson's ratio, subduction, and crustal structure in central Alaska. Journal of Geophysical Research 111. http://dx.doi.org/10.1029/2005JB003956 (B09311).
Sol, S., Meltzer, A., Burgmann, R., et al., 2007. Geodynamics of the southeastern Tibetan Plateau from seismic anisotropy and geodesy. Geology 35, 563–566.
Teng, J., Yin, Z., Liu, H., Zhang, Z., Hu, J., Sun, K., Wei, J., 1994. The 2D and 3D lithosphere structure and continental dynamics of Qinghai–Xizang Plateau. Chinese Journal of Geophysics 37, 117–130.
Thybo, H., 2006. The heterogeneous upper mantle low velocity zone. Tectonophysics 416, 53–79.
Wang, J., Huang, S., 1990. Compilation of heat flow data in the China continental area (2nd edition). Seismology and Geology 12, 351–366.
Wang, Q., Zhang, P., Freymueller, J., Bilham, R., Larson, K., et al., 2001. Present-day crustal deformation in China constrained by global positioning system measurements. Science 294, 574–577.
Wessel, P., Smith, W., 1998. New, improved version of Generic Mapping Tools released. Eos Trans. AGU 79, 579.
Wu, J., Zhang, Z., 2012. Spatial distribution of seismic layer, crustal thickness, and Vp/Vs ratio in the Permian Emeishan Mantle Plume region. Gondwana Research 22, 127–139.
Xu, T., Xu, G., Gao, E., Li, Y., Jiang, X., Luo, K., 2006. Block modeling and segmentally iterative ray tracing in complex 3D media. Geophysics 71, T41–T51.
Xu, T., Zhang, Z., Gao, E., Xu, G., Sun, L., 2010. Segmentally iterative ray tracing in complex 2D and 3D heterogeneous block models. Bulletin of the Seismological Society of America 100, 841–850.
Xu, Y., Yang, X., Li, Z., Liu, J., 2012. Seismic structure of the Tengchong volcanic area southwest China from local earthquake tomography. Journal of Volcanology and Geothermal Research 239–240, 83–91.
Yao, H., Beghein, C., Hilst, R.D., 2008. Surface wave array tomography in SE Tibet from ambient seismic noise and two-station analysis-II. Crustal and upper-mantle structure. Geophysical Journal International 157, 775–795.
Yao, Z., Roberts, R., Tryggvason, A., 1999. Calculating resolution and covariance matrices for seismic tomography with the LSQR method. Geophysical Journal International 138, 886–894.
Zhang, Z., Badal, J., Li, Y., Chen, Y., Yang, L., Teng, J., 2005. Crust-upper mantle seismic velocity structure across Southeastern China. Tectonophysics 395, 137–157.
Zhang, Z., Bai, Z., Mooney, W., Wang, C., Chen, X., Wang, E., Teng, J., Okaya, N., 2009. Crustal structure across the Three Gorges area of the Yangtze platform, central China, from seismic refraction/wide-angle reflection data. Tectonophysics 475, 423–437.
Zhang, Z., Yuan, X., Chen, Y., Tian, X., Kind, R., Li, X., Teng, J., 2010. Seismic signature of the collision between the east Tibetan escape flow and the Sichuan Basin. Earth and Planetary Science Letters 292, 254–264. http://dx.doi.org/10.1016/j.epsl.2010.01.046.
Zhang, Z., Klemperer, S., Bai, Z., Chen, Y., Teng, J., 2011. Crustal structure of the Paleozoic Kunlun orogeny from an active-source seismic profile between Moba and Guide in East Tibet, China. Gondwana Research 19, 994–1007.
Zhang, Z., Xu, T., Zhao, B., Badal, J., in press. Systematic variations in seismic velocity and reflection in the crust of Cathaysia: New constraints on intraplate orogeny in the South China continent. Gondwana Research. http://dx.doi.org/10.1016/j.gr.2012.05.018.
Zhao, L., 1993. Lateral variations and azimuthal isotropy of Pn velocities beneath basin and range province. Journal of Geophysical Research 98, 22109–22122.
Zhang, Z., Klemperer, S., 2010. Crustal structure of the Tethyan Himalaya, southern Tibet: new constraints from old wide-angle seismic data. Geophysical Journal International 181, 1247–1260. http://dx.doi.org/10.1111/j.1365-246X.2010.04578.x.